Marine Geoscience and Energy Resources 187 (2026) 207672

Contents lists available at ScienceDirect

Marine Geoscience and Energy Resources

journal homepage: www.sciencedirect.com/journal/marine-geoscience-and-energy-resources

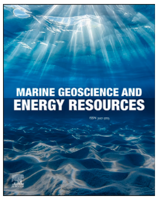

Introduction to the special issue: Application of sulphur compounds and isotopes to paleoenvironment and petroleum geology studies

Sulphur is an exceptionally powerful geological tracer because it spans a broad range of oxidation states and undergoes rapid redox cycling across the water column, sediments, and deep reservoirs. Accordingly, sulphur isotopes—most commonly $\delta^{34}S$ and, increasingly, multiple-sulphur isotope systematics—provide an integrated link between microbial metabolisms, sedimentary diagenesis, basin-scale fluid–rock reactions, and the preservation of both inorganic sulphides (e.g., pyrite) and organic sulphur compounds (OSCs). In palaeoenvironmental studies, $\delta^{34}S$ records are widely used to constrain sulphate availability, the balance between sulphate reduction and sulphide re-oxidation, and the efficiency of sulphide burial as pyrite. A key underpinning is the early-diagenetic framework in which pyrite formation is governed by reactant supply (sulphate, reactive iron, and degradable organic matter) and by kinetic pathways that convert dissolved sulphide into iron sulphides and ultimately pyrite (Berner, 1984).

Over the last decade, interpretations have shifted from “single-value proxy” approaches to process-based frameworks that explicitly consider non-steady-state diagenesis, variable sedimentation, and spatial heterogeneity in porewater reaction networks. Diagenetic modelling indicates that organic-carbon supply, sulphate transport and availability, and the delivery of reactive iron together control both the magnitude and isotopic expression of sulphide production and fixation (Mertens et al., 2025). This distinction is important because isotopically “heavy” (^{34}S-enriched) pyrite can form without invoking exotic sulphur sources: high sedimentation rates and non-steady-state deposition can drive porewater sulphate evolution and isotopic distillation, elevating pyrite $\delta^{34}S$ even in fully marine settings (Liu et al., 2021). Accordingly, pyrite $\delta^{34}S$ does not simply mirror “ocean redox”; it also reflects local boundary conditions (mass transport versus reaction rates) and sedimentological context.

Sulphur isotopes have also become central to methane-cycle reconstructions and interpretations of seep and gas-hydrate systems. At the sulphate–methane transition zone(s) (SMTZ/S), anaerobic oxidation of methane can couple with sulphate reduction to produce authigenic sulphides whose $\delta^{34}S$ values depend strongly on original sulphate $\delta^{34}S$ values, sulphate concentrations, Rayleigh-type distillation, and open- versus closed-system behaviour (Cai et al., 2022b). Consequently, ^{34}S-enriched authigenic sulphides have been proposed as indicators of elevated methane flux and gas hydrates in the geological record, but the signal is process-contingent and should be interpreted alongside sedimentation rate, sulphate replenishment, and mineralisation pathways (Borowski et al., 2013).

In petroleum geology, sulphur isotopes are widely used to diagnose thermochemical sulphate reduction (TSR), constrain H_2S sources, and track the generation and transformation of volatile and non-volatile OSCs. Because TSR can severely degrade petroleum quality and create major safety and corrosion challenges, reliable geochemical identification and staging of TSR remain high priorities (Cai et al., 2003, 2022a; Amrani, 2014). Recent syntheses emphasise advances in TSR reaction networks and isotope fractionation, alongside emerging proxies based on multiple-sulphur isotopes, compound-specific sulphur isotopes, and in situ SIMS/NanoSIMS approaches (Cai et al., 2023).

A recurring message across these application areas is that sulphur signals are rarely “single-process”: they integrate transport limitation, reaction kinetics, mixing, and multi-stage histories. Field observations and experiments are therefore essential for translating sulphur systematics into robust, operationally useful workflows for palaeoenvironmental reconstruction and petroleum-system evaluation.

This Special Issue of Marine and Petroleum Geology brings together 21 papers integrating sulphur isotopes, organosulphur compounds, pyrite petrography, and thermochemical experiments to address questions spanning the Ediacaran to the Holocene and black-shale deposition to ultra-deep sour-gas accumulations. The contributions fall into four thematic clusters: (1) sulphur compounds as tracers of gas origin, alteration, and souring; (2) pyrite-based proxies for palaeo-redox evolution and organic-matter enrichment; (3) maturation trends and experimental constraints on organosulphur behaviour; and (4) broader applications to ore formation and palaeoecology.

1. Sulphur compounds as tracers of gas origin, alteration and souring

Several papers illustrate the diagnostic value of volatile organosulphur compounds (VOSCs), the isotopic composition of H_2S, and heteroatom-rich NSO compounds for disentangling the origins and alteration histories of natural gases.

Wang et al. (2024) analyse $\delta^{34}S$ values of individual VOSCs in Tarim Basin gases (NW China) and related dibenzothiophenes (DBTs) in oils. VOSCs unaffected by TSR match Cambrian kerogen signatures, confirming a Cambrian gas source. Gas samples with anomalously ^{34}S-enriched VOSCs but no TSR fingerprints instead indicate mixing with exogenous TSR-derived H_2S. Their work highlights VOSCs as

---

This article is part of a special issue entitled: Sulfur geochemistry published in Marine Geoscience and Energy Resources.

https://doi.org/10.1016/j.marger.2026.207672

powerful, underutilised tracers for gas–source correlation and late-stage mixing.

Cai et al. (2025) examine H_2S generation during steam-assisted gravity drainage in the Bamianhe Oilfield (central China). Integrated gas–oil–water isotopic and molecular data reveal multiple H_2S pathways, including thermal cracking of organic matter, TSR, and bacterial sulphate reduction (BSR). VOSC assemblages effectively distinguish thermal-cracking alteration (organic matter cracking), TSR (thiophene-rich), aquathermolysis (thiols/sulphides with trace thiophenes), and BSR (thiol-poor and thiophene-free), providing operationally useful souring diagnostics.

In the Montney Formation (west-central Alberta, Canada), Wood and Biersteker (2025) show that high-H_2S zones exhibit strongly ^{13}C-enriched $\delta^{13}C$ values in ethane and propane, forming convex-upward Chung plots diagnostic of TSR. Lateral increases in $\delta^{13}C$ values of C_2–C_3, but not CH_4, confirm that ethane and propane are preferentially oxidised during TSR.

In shale reservoirs, Cui et al. (2025) document moderate but unexpected H_2S concentrations (0.3–2%) in Permian shales from Hubei. They rule out interlayer contamination and acid–rock reactions; sulphur isotope systematics and formation-water ion chemistry instead indicate fracturing-induced BSR, highlighting a previously underappreciated risk in shale-gas development.

For shale-oil allocation, Han et al. (2025) apply Fourier transform ion cyclotron resonance mass spectrometry (FT-ICR-MS) to hypersaline Qianjiang shales. Negative-ion NSO compounds and positive-ion aromatic sulphur species enable deconvolution of oils produced from commingled fractured intervals, accurately identifying the productive shale packages enriched in saturated hydrocarbons.

.

Finally, Souza et al. (2025) conduct gold-tube TSR experiments on lacustrine oil relevant to Brazilian pre-salt reservoirs. They derive kinetic parameters (activation energy $E_a = 53$ kcal mol^{-1}; pre-exponential factor $Af = 4.8 \times 10^{13}$ s^{-1}) and demonstrate substantial H_2S and CO_2 generation, progressive ^{13}C enrichment in $\delta^{13}C$ values of C_1–C_3 and CO_2, and convergence of $\delta^{34}S_{H2S}$ towards that of the initial sulphate. These parameters improve H_2S prediction in petroleum-system models.

2. Pyrite and sulphur as archives of redox evolution and organic-matter enrichment

Pyrite morphology and sulphur isotope ratios provide a second central theme, with multiple studies reconstructing redox structures across diverse lake and marine systems.

Zhao et al. (2025) show that Lower Cretaceous Dalazi Formation shales formed under anoxic, ferruginous lake conditions with limited sulphate supply. Low chemical index of alteration (CIA) values reflect minimal weathering input, and $\delta^{34}S_{py}$ values indicate restricted HS^- availability. Despite limited euxinia, sustained anoxic ferruginous conditions allowed exceptional organic-matter preservation.

In modern analogues, Gu et al. (2025) document framboidal pyrite with $\delta^{34}S_{py}$ values from −47 to −8 ‰, indicating large microbial sulphate reduction (MSR)-driven fractionations in Holocene Yellow Sea sediments. $\delta^{34}S_{py}$ profiles record transitions between open- and closed-system MSR linked to sedimentation and stratification.

The Triassic Chang 7 lacustrine system in the Ordos Basin receives detailed coverage. Liu et al. (2025) reconstruct basin-wide redox shifts and propose that the Chang 7^3 sub-member was deposited under dysoxic–anoxic conditions, enabling TOC up to 35 wt%. The Chang 7^2 sub-member shows fluctuating dysoxia–oxia, whereas Chang 7^1 records more oxygenated waters. These trends illuminate lacustrine ecological recovery after the end-Permian mass extinction. Ma et al. (2025) propose a mineral-based degree of pyritisation (DOPM) and show that fine, narrowly distributed framboids and low $\delta^{34}S_{py}$ correlate strongly with organic matter and hydrocarbon enrichment, providing predictive tools for shale-oil potential. Gan et al. (2025) report phosphatised embryo-like fossils preserved alongside small pyrite framboids and collophane; suboxic waters and phosphate-rich pore fluids facilitated permineralisation of resting eggs, linking redox fluctuations with exceptional fossil preservation and lake productivity.

At the Ediacaran–Cambrian boundary in Qiongzhusi Formation shales (eastern China), Xu et al. (2025) combine sulphur isotopes, pyrite textures, elemental geochemistry, and U–Pb ages to distinguish restricted, anoxic–sulphidic bottom waters in the Ziyang region from dysoxic, bioturbated conditions in the Jingyan region, explaining lateral TOC heterogeneity.

Fu et al. (2025) integrate pyrite-based proxies across shelf–slope–basin settings, revealing expansion of mid-depth euxinia into intraplatform basins during Cambrian Age 2–3, followed by widespread shelf oxygenation during Age 3 that coincided with early metazoan diversification. A platform-scale $\delta^{34}S$_py gradient reflects changing sulphate reservoirs and redox structure.

Extending into the Silurian, He et al. (2025) demonstrate extreme $\delta^{34}S$ heterogeneity (−31 to +69 ‰) among pyrite morphologies in the Longmaxi Formation using NanoSIMS. Framboids uniquely record coeval seawater sulphate, whereas euhedral and fossil-hosted pyrites reflect progressive diagenesis and TSR-like processes.

Sun et al. (2025) propose two models to explain extraordinarily high TOC (>3 wt%) in the Silurian Longmaxi Formation. In a "sedimentation rate–H_2S concentration" model, rapid burial and abundant ^{34}S-rich H_2S promote TOC maxima in inner-shelf settings. In a "Kwangsian Orogeny–restriction" model, tectonic uplift reduces sulphate supply, governing diachronous termination of high-TOC intervals.

In ultra-deep settings, Jia et al. (2025) show that Ordovician pyrite in the Ordos Basin evolved from MSR (Py1) to multi-stage TSR (Py2–Py4). Systematic increases in $\delta^{34}S$ and decreases in trace-metal concentrations track transitions from oil-dominated TSR to wet-gas-dominated TSR, demonstrating that pyrite can sensitively record hydrocarbon phase evolution.

Du et al. (2025) provide complementary insights from Upper Permian Longtan Formation coal systems: pyritic sulphur dominates, but large $\Delta^{34}S_{SO4\text{–}Spy}$ values indicate BSR as the principal control. Low $\delta^{34}S$ values of elemental sulphur reflect partial derivation from humic sulphur during thermal evolution.

Li et al. (2025) document unusual interlayered silicate–pyrite and silicate–siderite minerals in modern Shenhu hydrate-bearing sediments in the South China Sea, linking their formation to microbially mediated weathering of silicates driven by methane-rich fluids at and below the palaeo sulphate–methane transition zone.

Hu et al. (2025) reveal micrometre-scale $\delta^{34}S$ variability (up to 69 ‰) within single Ediacaran pyrite grains, attributable to rapid nucleation within a dynamically mixed sulphur pool. Their work underscores the need to integrate micro-scale isotopic information into palaeoenvironmental interpretations.

3. Organosulphur behaviour during maturation and experimental heating

Srinivasan et al. (2025) evaluate methyl-dibenzothiophene (MDBT) distributions during hydrous pyrolysis of Type II-S kerogen and oil and compare these with naturally matured samples. While MDBT ratios are reliable maturity indicators in natural systems, they behave inconsistently under closed-system hydrous pyrolysis because of sulphur buffering, limited temperature ranges, and matrix effects. Triaromatic steroids provide more consistent maturity trends. The study cautions against direct transfer of artificial pyrolysis indices to naturally evolved sulphur-rich systems.

4. Sulphur in ore formation and wider palaeoenvironmental implications

Beyond petroleum systems, Cheng et al. (2026) use biomarker and isotope data from Niujiaotang Formation Pb–Zn ores to show that Cambrian-derived, sulphur-rich hydrocarbons were key reductants driving TSR and generating H_2S essential for metal precipitation. Their work demonstrates how petroleum geochemistry and sulphur systematics can further illuminate the genesis of MVT ore deposits.

5. Outlook

Collectively, the contributions showcase the unique capacity of sulphur-focused analyses to bridge petroleum geochemistry, palaeoenvironmental reconstruction, microbial processes, and basin evolution. Across a wide variety of sedimentary and mineral settings, several unifying insights emerge:

a) Pyrite-based proxies should be interpreted through a multi-generational lens, integrating framboidal and diagenetic/TSR pyrite populations.
b) Organosulphur compounds—including VOSCs and NSO species—provide high-resolution fingerprints of gas origin, reservoir alteration, and producing-interval allocation.
c) Experimental constraints on TSR kinetics and organosulphur maturation are essential for reliable H_2S prediction in deep and pre-salt systems.
d) Sulphur proxies illuminate major evolutionary and ecological transitions, from Cambrian ocean oxygenation to Triassic lacustrine productivity.

We anticipate that integrating in situ sulphur isotope imaging, advanced mass spectrometry, and reactive-transport modelling will further expand sulphur's role as a central geochemical tool linking Earth history and petroleum-system processes.

References

Amrani, A., 2014. Organosulphur compounds: molecular and isotopic evolution from biota to oil and gas. Annu. Rev. Earth Planet Sci. 42, 733–768.

Berner, R.A., 1984. Sedimentary pyrite formation: an update. Geochem. Cosmochim. Acta 48, 605–615.

Borowski, W.S., Rodriguez, N.M., Paull, C.K., Ussler III, W., 2013. Are ^{34}S-enriched authigenic sulfide minerals a proxy for elevated methane flux and gas hydrates in the geologic record? Mar. Petrol. Geol. 43, 381–395.

Cai, C.F., Liu, D.W., Hu, Y.J., Huang, T.Y., Jiang, Z.W., Xu, C.L., 2023. Interlinked marine cycles of methane, manganese, and sulfate in the post-Marinoan Doushantuo cap dolostone. Geochim. Cosmochim. Acta 346, 245–258.

Cai, C.F., Lyons, T.W., Sun, P., Liu, D., Wang, D., Tino, C.J., Luo, G., Peng, Y., Jiang, L., 2022b. Enigmatic super-heavy pyrite formation: novel mechanistic insights from the aftermath of the Sturtian Snowball Earth. Geochem. Cosmochim. Acta 334, 65–82.

Cai, C.F., Tian, Q.Z., Zhang, Z.X., 2022a. Thermochemical sulphate reduction in sedimentary basins and beyond: a review. Chem. Geol. 607, 121018.

Cai, C.F., Worden, R.H., Bottrell, S.H., Wang, L.S., Yang, C.C., 2003. Thermochemical sulphate reduction and the generation of hydrogen sulphide and thiols (mercaptans) in Triassic carbonate reservoirs from the Sichuan Basin, China. Chem. Geol. 202, 39–57.

Cai, S., Xiao, Q., Yang, X., 2025. Geochemical constraints on the genetic pathways of hydrogen sulfide in the Bamianhe Oilfield of Bohai Bay Basin, China. Mar. Petrol. Geol. 178, 107422.

Cheng, Y., Zhou, J.-X., Hu, Y., Xu, S., Shig, S., Wen, Y., Nie, Q., Zhou, Y., Luo, K., Tang, X., Zhou, L., Li, Y., Liu, Y., Zhang, X., 2026. The biomarker signatures in the Niujiaotang sulfide orefield: exploring the role of organic matter in ore formation. Mar. Petrol. Geol. 183, 107616.

Cui, Y., Li, L., Yang, H., Pan, K., Xin, J., Hu, Y., Peng, X., Yang, F., 2025. Origin of hydrogen sulfide in produced gas of upper Permian shale from western Hubei, southern China: a preliminary study. Mar. Petrol. Geol. 182, 107570.

Du, S., Long, E., Qi, Y., Ju, Y., Wu, P., Fu, Y., Gu, S., Zhang, H., Li, Q., 2025. The evolution of sulphur during coalification in marine land interaction environments based on the sequential extraction of different sulphur species. Mar. Petrol. Geol. 173, 107266.

Fu, F., Zou, C., Zhao, Z., Pan, S., Wang, W., Luo, C., Hua, G., Lu, G., Yuan, M., Yin, J., Jing, Z., 2025. Oceanic redox variations during the Cambrian Age 2–3 in the Yangtze Block of South China: evidence from pyrite-based proxies. Mar. Petrol. Geol. 179, 107438.

Gan, D., Dong, J., Yang, W., Liu, W., Gao, T., Wang, J., Bian, C., Xie, L., Li, Y., Liu, J., Hua, H., Liu, L., 2025. Phosphatized embryo-like fossils from the Chang 73 member, middle-upper Triassic Yanchang Formation, Ordos Basin, northwest China: affinity, preservation and paleoecological implications. Mar. Petrol. Geol. 181, 107531.

Gu, Y., Chang, X., Liu, X., Zhang, M., An, Y., Zhuang, G., Wang, H., 2025. Geochemical insights into authigenic pyrite formation in central Yellow Sea sediments: influence of sedimentary environment and microbial sulphate reduction. Mar. Petrol. Geol. 182, 107587.

Han, Y., An, D., Wu, S., Wang, F., Guo, X., He, Z., 2025. Oil–reservoir correlation: unravelling the producing reservoir for the sulphur-rich Qianjiang shale oil play. Mar. Petrol. Geol. 171, 107176.

He, K., Ye, Y., Wang, X., Chen, Y., Lei, Q., Yang, C., Zhang, S., 2025. Multigenetic origins of pyrite in sedimentary systems: a NanoSIMS sulphur isotope study of the Silurian Longmaxi Formation. Mar. Petrol. Geol. 178, 107423.

Hu, Y., Wang, W., Zhao, X., Guan, C., Zhou, C., Song, C., Shi, H., Sun, Y., Chen, Z., Yuan, X., 2025. Extreme sulphur isotope heterogeneity in individual Ediacaran pyrite grains revealed by NanoSIMS analysis. Mar. Petrol. Geol. 171, 107201.

Jia, L., Qin, B., Ma, C., Zheng, R., Zhang, J., 2025. Genesis and geological significance of pyrite in the Ordovician carbonate-evaporative strata of central Ordos Basin, China. Mar. Petrol. Geol. 182, 107586.

Li, Y., Lu, X., Huang, X., Lu, H., 2025. Occurrence and formation mechanism of silicate-interlayer iron minerals in hydrate-bearing sediment. Mar. Petrol. Geol. 173, 107265.

Liu, H., Huang, Y., Zhao, X., Wang, W., Qiu, X., Qiu, Z., Han, J., Shen, Z., Li, Y., Hua, G., Chen, Z.-Q., Zou, C., 2025. Temporal and spatial variations of redox conditions in the middle Triassic Chang 7 member of the Yanchang formation, Ordos Basin, North China. Mar. Petrol. Geol. 182, 107565.

Liu, J., Antler, G., Pellerin, A., Izon, G., Dohrmann, I., Findlay, A.J., Røy, H., Ono, S., Turchyn, A.V., Kasten, S., Jørgensen, B.B., 2021. Isotopically "heavy" pyrite in marine sediments due to high sedimentation rates and non-steady-state deposition. Geology 49, 816–821.

Ma, B., Ji, L., Zhou, Q., Zhang, Y., Fu, S., Xiao, Y., Sun, H., 2025. Morphology and sulphur isotopes of pyrite in Chang73 shale: indications for redox conditions and enrichment of organic matter and hydrocarbons. Mar. Petrol. Geol. 180, 107484.

Mertens, G., Paradis, E., Hemingway, J.D., Halevy, I., 2025. Sedimentary conditions drive modern pyrite burial flux to exceed oxidation. Nat. Geosci. https://doi.org/10.1038/s41561-025-01855-5.

Souza, I., Tang, Y.C., Lu, L., Ferreira, A.A., Ellis, G.S., Díaz, R.A., Carvalho, L.F., Coutinhoe, Albuquerque, A.L.S., 2025. Kinetics of thermochemical sulphate reduction based on pyrolysis gold-tube experiments on lacustrine oil: implications for H_2S prediction in Brazilian pre-salt reservoirs. Mar. Petrol. Geol. 182, 107600.

Srinivasan, P., Sandu, C., Endara Arguello, E.M., Atwah, I., 2025. Inconsistencies in Organosulphur compounds during natural and artificial maturation. Mar. Petrol. Geol. 182, 107541.

Sun, Z., Chen, H., Lang, X., Zhang, B., Chen, Q., Zhao, K., Zhu, S., Zhao, F., Liang, F., Liu, C., Fan, J., 2025. Mechanisms for initiation and termination of extraordinarily high total organic carbon in the longmaxi Formation, Yangtze platform, south China. Mar. Petrol. Geol. 182, 107588.

Wang, D., Kutuzov, I., Zhang, H., Cao, Z., Wang, Q., Amrani, A., Cai, C., 2024. Application of sulphur isotopes of volatile organic sulphur compounds to determine the natural gas secondary alterations and possible sources in the Tarim Basin, NW China. Mar. Petrol. Geol. 169, 107078.

Wood, J.M., Biersteker, V., 2025. δ^{13}C signatures of a natural gas zone with high H_2S content in a major unconventional petroleum accumulation, Montney Formation, western Canada. Mar. Petrol. Geol. 180, 107482.

Xu, H., Shen, J., Deng, H., Yang, F., Hu, Q., Yu, Y., Xiong, L., Zhang, T., Deng, H.C., He, J. H., 2025. Provenance, sedimentary paleoenvironment and organic matter accumulation mechanisms in shales from the Lower Cambrian Qiongzhusi Formation, SW Yangtze Block, China. Mar. Petrol. Geol. 181, 107520.

Zhao, X., Wang, W., Liu, H., Hu, Y., Zhao, X., Song, C., Guan, C., Zheng, D., Zhang, H., 2025. Depositional environments of the organic-rich shales from the Lower Cretaceous Dalazi Formation in the Yanji and Luozigou Basins of Northeast China. Mar. Petrol. Geol. 179, 107437.

Chunfang Cai[a,*], Paul Greenwood[b,c], Bernhard Mayer[d], Xianguo Lang[e], Wei Wang[f]

[a] *National Key Lab Petroleum Resource & Engineering, China University of Petroleum, Beijing, 102249, China*
[b] *Western Australia Organic and Isotope Geochemistry Group, Curtin University, Perth, Western Australia, Australia*
[c] *School of Earth Sciences, University of Western Australia, Perth, Western Australia, Australia*
[d] *University of Calgary, Calgary, Alberta, Canada*
[e] *Chengdu University of Technology, Chengdu, China*
[f] *Nanjing Institute of Geology and Palaeontology, Chinese Academy of Sciences, Nanjing, China*

[*] Corresponding author.
E-mail address: cai_cf@cup.edu.cn (C. Cai).